Semiconductor Science and Technology

PAPER

Low voltage & controlled switching of MoS_2-GO resistive layers based ReRAM for non-volatile memory applications

To cite this article: Sumit Choudhary *et al* 2019 *Semicond. Sci. Technol.* **34** 085009

IOP Publishing Semiconductor Science and Technology
Semicond. Sci. Technol. 34 (2019) 085009 (11pp) https://doi.org/10.1088/1361-6641/ab2c09

Low voltage & controlled switching of MoS_2-GO resistive layers based ReRAM for non-volatile memory applications

Sumit Choudhary, Mahesh Soni and Satinder K Sharma

School of Computing and Electrical Engineering (SCEE), Indian Institute of Technology (IIT) Mandi, MANDI-175005 (Himachal Pradesh), India

E-mail: satinder@iitmandi.ac.in

Received 23 March 2019, revised 4 June 2019
Accepted for publication 24 June 2019
Published 16 July 2019

Abstract

Emerging information technology and data deluge foster the unprecedented demands of higher chip density, clocking speed, data storage and lower power dissipation for on-chip non-volatile memories (NVMs). Here, two types of metal-insulator-metal (MIM) based NVM structures were fabricated and demonstrated involving controlled functionalization of molybdenum disulfide (MoS_2) and graphene oxide (GO) nanocomposite as a resistive switching layer. The first type of device constitutes Aluminum (Al) top and bottom electrode resulting in the Al/MoS_2-GO/Al structure. While the second type of device uses Al top electrode and Indium Tin Oxide (ITO) bottom electrode resulting in Al/MoS_2-GO/ITO. The current-voltage (I–V) characteristics for fabricated Al/MoS_2-GO/Al and Al/MoS_2-GO/ITO MIM structures exhibited considerable I_{ON}/I_{OFF} ratio of $\sim 10^2$ (SET and RESET state at 0.5 V and −0.4 V) and $\sim 10^1$ (SET and RESET state at 0.3 V and −1 V), respectively. The I–V characteristics for Al/MoS_2-GO/Al MIM structure showed low voltage switching, substantial memory retention $\sim 10^4$ s and endurance for up to 25 cycles. The low voltage and controlled switching operation for Al/MoS_2-GO/Al MIM structures may be attributed to the presence of a large number of oxygen vacancies, defects in MoS_2-GO, promoting enhanced charge hopping via interfacial oxide at MoS_2-GO/Al interface as compared to MoS_2-GO/ITO.

Keywords: resistive random-access memory, MoS_2-GO, conduction mechanism, emerging non-volatile memory

(Some figures may appear in colour only in the online journal)

Introduction

Recently, resistive random access memory (ReRAM) has attracted immense attention as a potential candidature for emerging non-volatile memory (NVM) devices largely motivated from its low operating power, higher speed, packing density and scalability [1, 2]. While, other memories including the phase-change random access memory, ferroelectric random access memory, magnetoresistive random access memory have been extensively researched for better scalability and low power operation [3, 4]. Among all, the ReRAM structure comprising of an active resistive switching (RS) layer sandwiched between two metal electrodes forms the metal insulator metal (MIM) system are attractive and widely studied due to following reasons [4, 5]. Firstly, ReRAM offers high speed and consumes low power during read and write operations [5]. Secondly, the ReRAM device structure makes it easy to realize multi-bit storage. The ReRAM based multi-bit design requires less number of hardware to store a similar amount of data/information as compared with the traditionally used CMOS based Boolean-logic devices [6–8]. Lastly, the RS layer realizes a computation-in-memory design, which reduces the energy needed for transporting data between memory and computing units [9, 10]. Even though, there are some critical device physics and processing-based concerns for RS layer-based ReRAM, which hinder its application and adaptation in next-generation electronics.

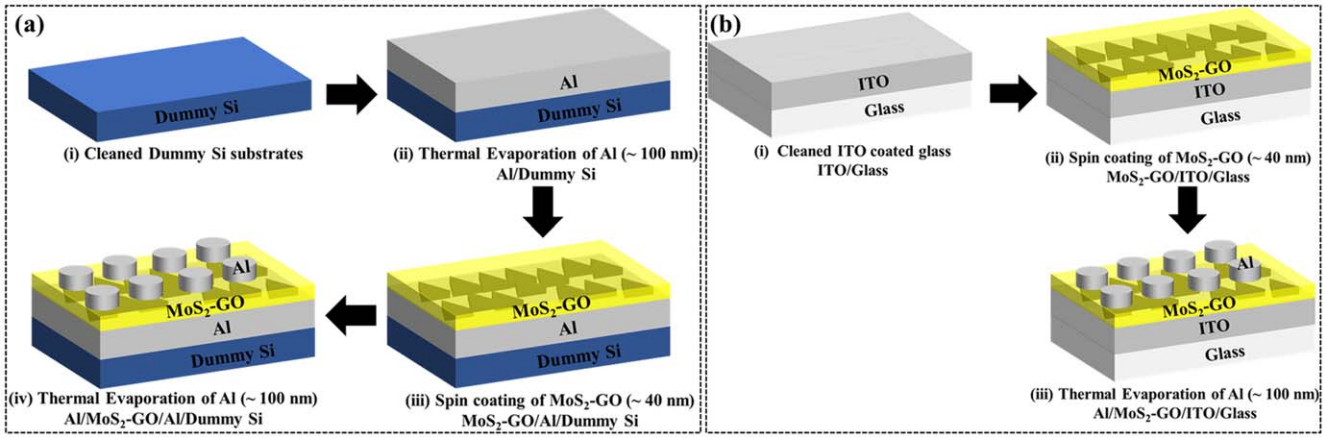

Figure 1. Schematic process steps for the fabrication of MoS_2-GO nanocomposite based ReRAM (a) Al/MoS_2-GO/Al/Dummy Si and (b) Al/MoS_2-GO/ITO/glass.

Typically in resistive memory based MIM devices, the switching action solely occurs onto the defect-free quality of transition metal oxides as a function of an applied electric field [11]. Recently graphene oxide (GO) [12, 13], perovskites [14], chalcogenides [15] and ferroelectrics [16] are also considered as a possible alternative of transition oxides. While, the latest report indicates that the active layer conduction mechanism is the drift of ionic species, result in the formation/rupturing of conductive filament (CF), [12] trapping de-trapping of charge species [17] and Fowler–Nordheim tunnelling [18].

Furthermore, the ultra-thin two dimensional (2D) materials such as graphene and its derivatives, transition metal dichalcogenides, for instance, molybdenum disulfide (MoS_2), titanium disulfide, tungsten disulfide, tantalum sulfide are also widely researched [19, 20]. In particular, 2D nanomaterials like MoS_2 and GO has drawn significant attention of scientific community because of distinctive physical, electronic properties, high flexibility, low cost, easy fabrication and 3D stacking capability [21]. As established, the bulk MoS_2 possesses an indirect band gap of ~1.2 eV, while, the monolayer shows direct band gap of ~1.8 eV [22] and the stacked monolayers of MoS_2 are connected with weak van der Waal forces [23]. The covalent bonds of sulphur (S) and molybdenum (Mo) atoms are spaced ~6.5 Å form the stacked planes of MoS_2 [24]. Whereas, the insulating GO surrounded by hydrophilic oxygen-rich functional groups shows the enormous potential in fast response memory & high-density integrations [25, 26]. Moreover, the functionalization of MoS_2 nanosheets with GO shows the resistive switching characteristics, can be utilized as an active layer for ReRAM [21]. Especially, the resistive memory with MoS_2-GO as an active resistive layer may have the potential for flexible electronics [7, 12]. This enables low-cost fabrication, high packing density, energy-efficient NVMs devices for future electronics.

In this work, MoS_2-GO nanocomposite functioning as an active resistive layer for the fabricated ReRAM structures was deposited by a controlled solution process. Here, two different types of ReRAM structures were fabricated in order to study the effect of metal electrodes on the performance of the devices. For the first type of device, the top and bottom electrodes were of Al, while for the second type of device, the bottom electrode was ITO and the top electrode was Al. Micro-Raman, energy dispersive x-ray spectroscopy (EDAX), cross-sectional field emission scanning electron microscopy (FESEM) and atomic force microscope (AFM) analysis on the active MoS_2-GO nanocomposite layer were performed to study the compositional, cross-sectional morphology/physical interface and surface properties. The current-voltage (I–V) measurements were performed to investigate the effect of the switching behaviour of Al/MoS_2-GO/Al and Al/MoS_2-GO/ITO structures. The retention and endurance of the device were measured to establish the reliability and feasibility of devices for real-world applications. Also, based on the obtained characteristics a switching mechanism was proposed using valence change supported by the migration of oxygen ions/vacancies to support the devices observations [27–29].

Experimental: fabrication of resistive memory device

The process schematic for the fabrication of two types of ReRAM devices is as shown in figure 1. Figure 1(a) presents the process steps followed for the fabrication of the 1st type of ReRAM device (Al/MoS_2-GO/Al/Dummy Si). While figure 1(b) shows the process steps for the fabrication of the 2nd batch of ReRAM device (Al/MoS_2-GO/ITO/Glass). For the 1st type, a square test grade dummy Si substrate (1 cm × 1 cm) was cleaned using standard RCA cleaning (as shown in figure 1(a, i)). Thereafter, the samples were subjected to bottom Al electrode deposition on cleaned dummy Si substrate using thermal evaporation at a vacuum of 10^{-6} mbar (as shown in figure 1(a, ii)). The thickness of the deposited Al film was found to be ~100 nm using NanoMap–LS (AEP Technologies, USA) stylus profilometer. For the 2nd type of ReRAM devices, ITO coated glass (ITO/glass) purchased from (Sigma Aldrich) resistivity of 8–12 Ω/sq was

used. The ITO/Glass substrate (1 cm × 1 cm) were cleaned by dipping the samples in boiling acetone for 15 min followed by dipping in fresh acetone, isopropyl alcohol (IPA) for 15 min each, N_2 air purging and dehydration bake on a hot plate at 100 °C for 30 min (figure 1(b, i)).

The functionalization of MoS_2 flakes with GO was easily accomplished by the direct ultra-sonication method. GO was synthesized using a modified Hummers method as described in our previous reports [30–32]. The MoS_2 powder (purchased from Sigma Aldrich) was dispersed in N-Methyl-2-pyrrolidone (NMP) at a concentration of 1.0 mg ml^{-1} under mild sonication (Frequency 33 KHz) for 2 h. Similarly, the synthesized GO powder was re-dispersed in the DI water at a concentration of 1.0 mg ml^{-1}. The MoS_2 dispersion in NMP was then added to the aqueous GO solution in the ratio of 1:1 under constant stirring for 4 h followed by sonication of MoS_2-GO for 2 h. Afterwards, the MoS_2-GO dispersion was centrifuged at 5000 rpm for 10 min and the final supernatant was collected and utilized for the fabrication of devices. A thin layer of the MoS_2-GO solution was deposited on Al/Dummy Si and ITO/glass substrates using spin-coating at 500 rpm for 1 min with the acceleration of 250 rpm s^{-1} immediately followed by spinning at 1000 rpm for 1 min with the acceleration of 500 rpm s^{-1}. The MoS_2-GO/Al/Dummy Si and MoS_2-GO/ITO/glass samples were then baked on a hot plate at 60 °C for 5 min. The similar spin coating procedure was used for both the devices in order to achieve a uniform and pin-hole free MoS_2-GO film with a thickness of ∼40 nm measured using NanoMap–LS (AEP Technologies, USA) as shown in figures 1(a, iii) and (b, ii).

The samples (MoS_2-GO/Al/Dummy Si and MoS_2-GO/ITO/glass) were then loaded into the thermal evaporator for the top metal contact. Circular Al electrodes thickness ∼100 nm measured using NanoMap–LS (AEP Technologies, USA) with an area of 600 um^2 and a diameter of ∼27 μm was deposited using a shadow mask at high vacuum 10^{-6} mbar to form Al/MoS_2-GO/Al/Dummy Si and Al/MoS_2-GO/ITO/glass, shown in figures 1(a, iv) and (b, iii), respectively. During the top electrode deposition, the slow evaporation of Al was preferred in order to avoid the well-known Al spiking issue [33]. The electrical characterizations of the fabricated devices were carried out using KEITHLEY 4200 SCS system attached to a cascade probe station. Here, in total 10 devices for each type of ReRAM structures (Al/MoS_2-GO/Al/Dummy Si and Al/MoS_2-GO/ITO/glass) were fabricated, out of which 7–8 devices demonstrated similar electrical characteristics. The surface and chemical analysis were recorded using Dimension Icon (AFM) from Bruker and Horiba LabRAM based micro–Raman Spectroscopy, respectively at room temperature.

Results and discussion

To measure the I–V characteristics on the fabricated ReRAM devices, sweeping voltages were applied on the top electrode keeping the bottom electrode grounded as shown in figure 2(a). Here, resistive memory behaviour can be described with the SET and RESET switching voltages. The voltage at which device switches from high resistance state (HRS) to low resistance state (LRS) (OFF to ON state) is termed as SET voltage. Whereas, the voltage at which device switches from LRS to HRS (ON to OFF state) is the RESET voltage. Figure 2(b), shows Al/MoS_2-GO/Al resistive memory switching states designated by arrows and numbers. For example, state '2' and state '5' represents the SET and RESET condition respectively, while respective HRS and LRS are represented by state '1' & '6' and state '3' & '4' respectively.

Here, dual mode voltage sweep was used for characterization of fabricated MIM structures. Initially, when a voltage is swept from 0 V to 0.5 V the device was in HRS (state '1') with a current value of $\sim10^{-6}$ A as shown in figure 2(b). It can clearly be seen from the figure 2(b), that for Al/MoS_2-GO/Al device at 0.5 V the current increases to $\sim10^{-4}$ A and the device approaches the SET condition, switching from HRS to LRS (demarcated as a state '2'). When the voltage is swept in the reverse direction from 0.5 V to 0 V to −0.5 V (state '3' and state '4', figure 2(b)) the Al/MoS_2-GO/Al device remembers its last state, i.e. LRS. When voltage sweep approaches at −0.35 V, the current shoots down to $\sim10^{-6}$ A, and the device reached the RESET state '5' (transition from LRS to HRS), as shown in figure 2(b). Finally, when the voltage is swept from −0.5 V to 0 V, the device retains the last state (HRS), shown as a state '6' in figure 2(b). While performing the I–V measurements, current compliance of 10 mA was used in order to prevent the permanent breakdown/failure of the devices.

Both sets of devices exhibit compliance-free behavior. With the applied bias, the randomly distributed oxygen vacancies in the MoS_2-GO layer are aligned, leading to the formation or disruption of filament. Under positive applied bias, once the filament is formed, it does not tend to scale in size. Therefore does not allow to further increase the current, leading to a self-stop at some resistance state results in compliance free switching [34]. Another possible reason for compliance free switching in MoS_2-GO ReRAM structures may be due to intrinsic built-in parasitic resistance of the filament [34, 35]. The research in ReRAM is moving forward to self-compliance approach to reduce the complexity of the circuit design as per the recent reports by [8, 35, 36]. For better understanding, evaluation of memory performance (for instance SET/RESET voltages and I_{ON}/I_{OFF} ratios) and comparison, the linear I–V characteristics of Al/MoS_2-GO/Al devices (figure 2(b) were plotted in semilogarithmic (log(I) versus (V)) scale as shown in figure 3(a). A similar methodology was also adopted to characterize Al/MoS_2-GO/ITO devices. I–V characteristics for Al/MoS_2-GO/ITO structures with different states (labelled '1'–'6') are as shown in figure 3(b).

For Al/MoS_2-GO/Al, devices SET and RESET voltages were measured ∼0.5 and ∼−0.35 V, respectively and I_{ON}/I_{OFF} current ratio was $\sim10^2$ (figure 3(a)). In contrast, Al/MoS_2-GO/ITO devices demonstrated SET and RESET voltages at ∼0.3 V and ∼−1 V respectively along with I_{ON}/I_{OFF} current ratio ∼10 (figure 3(b)). As clear from the

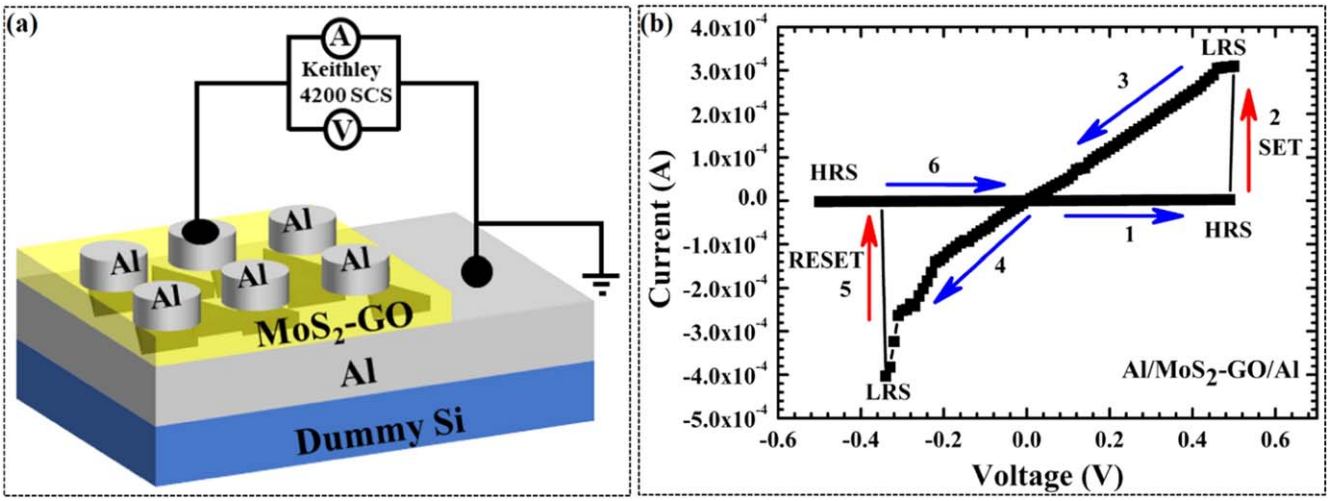

Figure 2. (a) MoS_2-GO nanocomposite 40 nm resistive layer devices with electrical characterization setup (b) Resistance switching states of Al/MoS_2-GO/Al (MIM) devices.

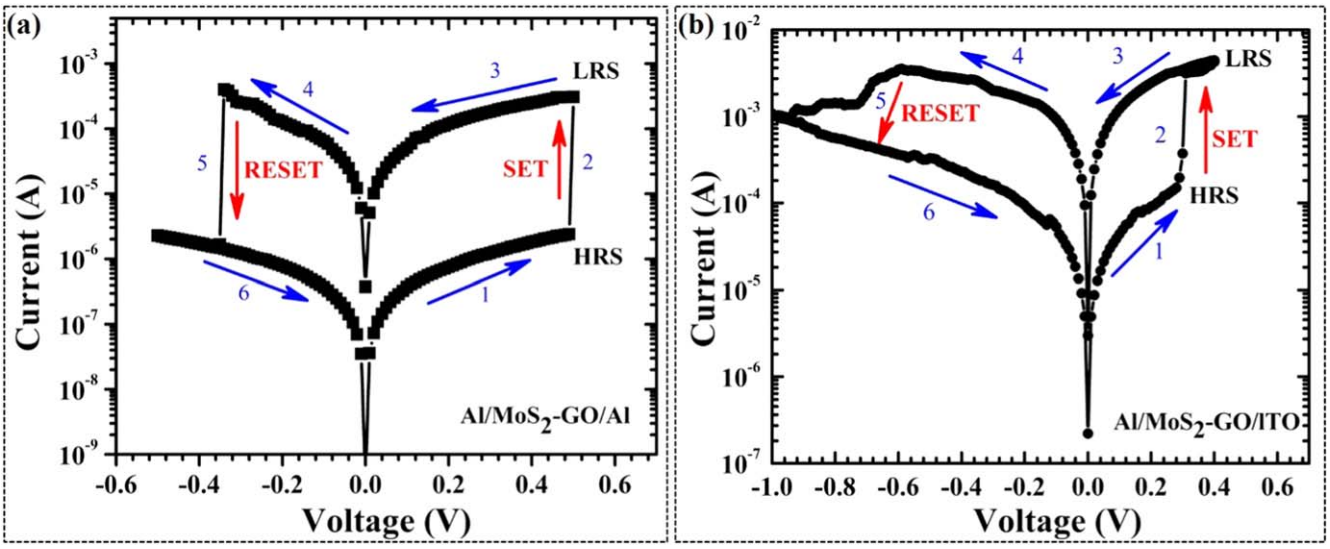

Figure 3. IV characteristics of (a) Al/MoS_2-GO/Al Metal Insulator Metal (MIM) devices (b) For Al/MoS_2-GO/ITO (MIM) devices.

figure 3(b), for up to −1 V, the Al/MoS_2-GO/ITO devices show no abrupt current switching and current is varying gradually with the voltage sweep during the RESET process. It may be due to the instability of CF. The characteristics of Al/MoS_2-GO/Al devices shows controlled SET and RESET behavior and I_{ON}/I_{OFF} current ratio was found to be ∼one order higher as compared to Al/MoS_2-GO/ITO devices. The high I_{ON}/I_{OFF} ratio in the Al/MoS_2-GO/Al devices may be attributed to increasing in defects/oxygen vacancies at the Al electrode interface, similar work reported in the past by Li *et al* [37]. Also, it is clear from figures 3(a) and (b), that both the devices (Al/MoS_2-GO/Al and Al/MoS_2-GO/ITO) demonstrated bipolar resistive switching behaviour. As compared to Al/MoS_2-GO/ITO, the enhanced memory performances (high I_{ON}/I_{OFF} ratio and stable SET/RESET) for Al/MoS_2-GO/Al may be attributed to the presence of highly oxidizable Al/GO interface and formulation of aluminium oxide (AlO_x) [38]. The interfacial AlO_x serves as a source of active oxygen dislocations, defects, resulting in the formation of CF in the resistive layer [39]. The performance comparison of the fabricated MoS_2-GO structures in the present work with the previously reported structures is summarized in table 1.

Moreover, there are various conduction mechanisms on resistive switching of oxides layers are reported in the literature; like aligned CF formed by the redox reaction of the electrochemically active electrode and valence change supported by the migration of oxygen ions/vacancies in the active layer [28, 46–51]. Thus, in Al/MoS_2-GO/Al and Al/MoS_2-GO/ITO MIM structures, CF formation/dissolution due to oxygen vacancy/ion migration under the applied external field is more applicable due to the presence of oxygen-rich MoS_2-GO layer. The pictorial view of the resistance switching mechanism is depicted in figure 4. Figures 4(a), (c) shows the formation of oxygen vacancy conducting filament. The dissolution of CF under the reverse electric field is

Table 1. The comparison of present work with the reported in the literature.

Active layer	Electrode	Thin film Fabrication Method	Switching Voltage	I_{ON}/I_{OFF} Ratio	Retention	Reference
GO	Top: Al Bottom: Al	Spin-coating	$\sim$2.5 V	$\sim10^2$	$>10^5$ s	[12]
GO	Top: Al Bottom: ITO	Spin-coating	$\sim$2.0 V	$\sim10^3$	—	[40]
rGO	Top: Al Bottom: ITO	Spin-coating	$\sim$5 V	$\sim10^3$	10^5 s	[41]
GO	Top: Cu Bottom: Pt	Vacuum filtration	$<$1 V	$\sim$20	10^4 s	[42]
Mixture of MoS_2 and GO sheets	Top: Al Bottom: ITO	Spin-coating	$<$1.5 V	$\sim10^2$	—	[43]
MoS_2–P123 hybrid nanofibers	Top: rGO Bottom: rGO	Spin-coating	3–4 V	$\sim5.5 \times 10^2$	4×10^3 s	[44]
PVP-coated MoS_2 sheets	Top: Al Bottom: rGO	Spin-coating	$\sim$3.5 V	$\sim10^2$	—	[45]
MoS_2-GO Nanocomposite	**Top: Al Bottom: Al**	**Spin-coating**	**$\sim$0.5 V**	**$\sim10^2$**	**$> 10^4$ s**	**This work**
MoS_2-GO Nanocomposite	**Top: Al Bottom: ITO**	**Spin-coating**	**$\sim$1 V**	**$\sim10^1$**	**$>10^4$ s**	**This work**

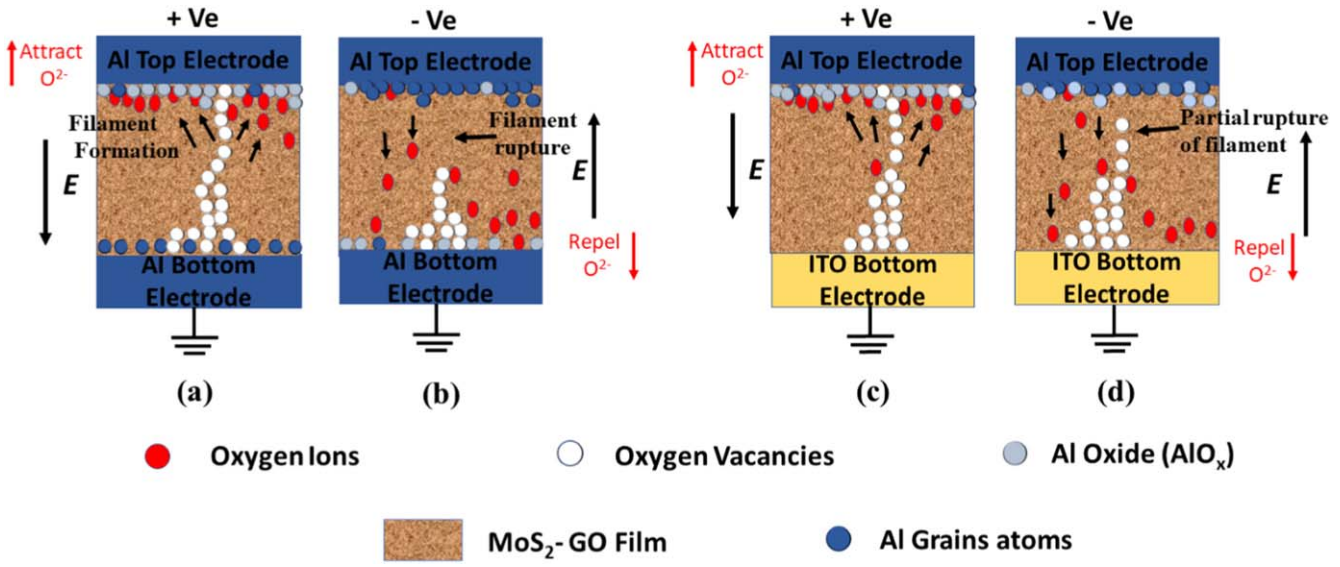

Figure 4. Depicts the CF-type conduction mechanism in Al/MoS_2-GO/ITO and Al/MoS_2-GO/Al devices. (Individual region dimensions are not to scale.)

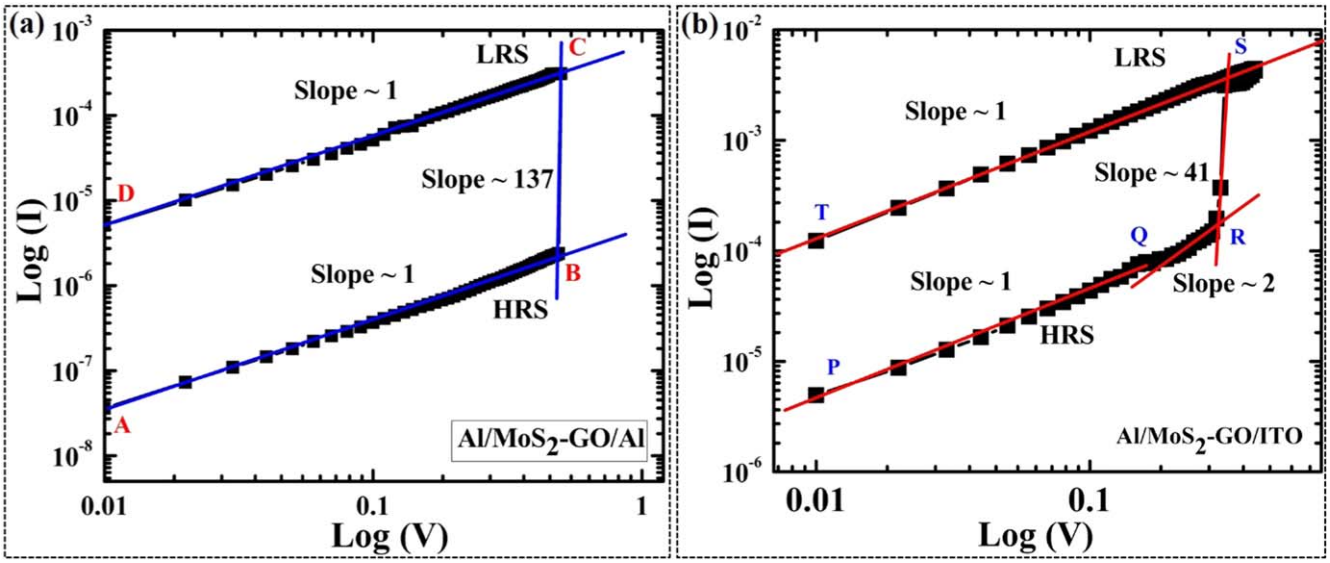

Figure 5. Double logarithm graphs of IV curves were plotted for (a) Al/MoS_2-GO/Al and (b) Al/MoS_2-GO/ITO devices at room temperature (298 °K).

represented by figures 4(b), (d). Figures 4(a), (b) shows the formation of unstable oxide (AlO_x) at the electrodes and nanocomposite MoS_2-GO interface. As discussed earlier, both the devices will remain in the HRS (RESET/OFF state) under no applied bias. When the positive bias (+Ve) is applied on the top (Al) electrode, the oxygen ions (O^{2-}) are drifted in the upward direction (as shown by an upward arrow in figures 4(a) and (c)) leaving behind oxygen vacancies in the MoS_2-GO layer. These vacancies form the oxygen-deficient filament, which is conducting in nature, acts as a virtual cathode, resulting in an increased current. Thus, turns 'ON' the device (SET condition) and the device approaches the LRS. Due to a variable electric field, oxygen vacancy concentration and localized temperature the CF formed is dynamic in nature (figures 4(a) and (c)). Locally formed filament grows towards the anode and distributed in the MoS_2-GO resistive layer [46, 47, 49, 52]. Alternatively, when a negative bias (−Ve) is applied on the top electrode, the oxygen ions migrate towards the bottom electrode (represented by a downward arrow in figures 4(b) and (d)) and recombine with conducting oxygen vacancies, this leads to the dissolution of conducting filament and results into RESET (LRS to HRS). The widespread alignment of oxygen vacancies; also results in the formation of a conductive path on applied external stimulus consequences the abrupt SET and while random/partial rupture of filament occurs on reverse stimulus outcomes in gradual RESET switching characteristics (figure 3(b)). Switching mechanism of the device is

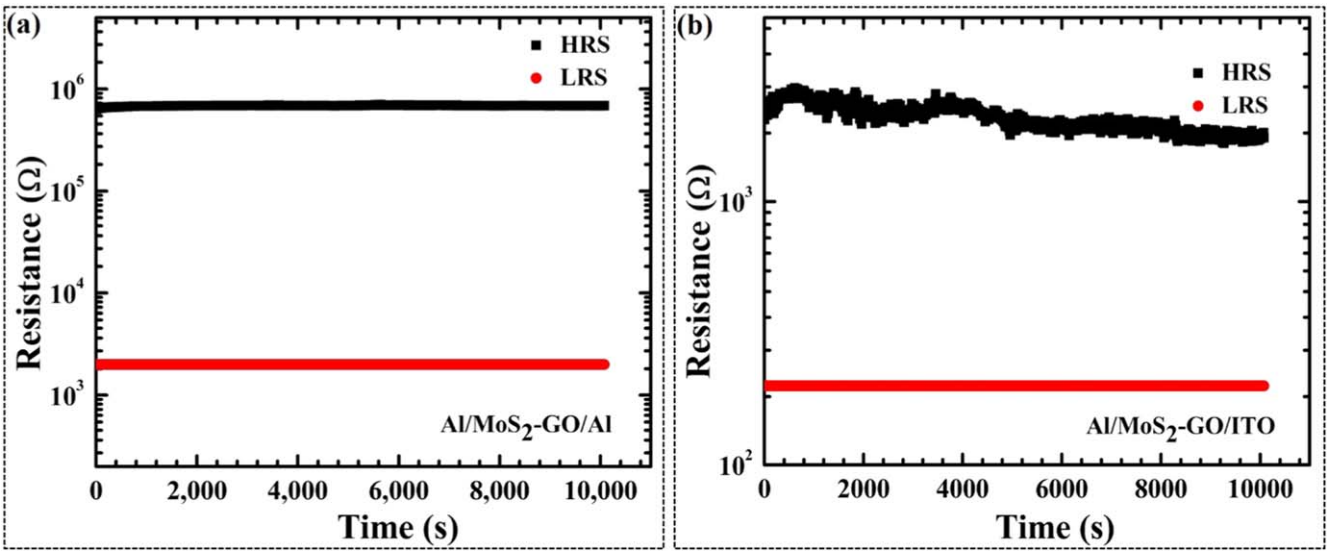

Figure 6. (a) and (b) shows the retention characteristics of Al/MoS_2-GO/Al and Al/MoS_2-GO/ITO devices respectively under a constant readout voltage of 0.2 V.

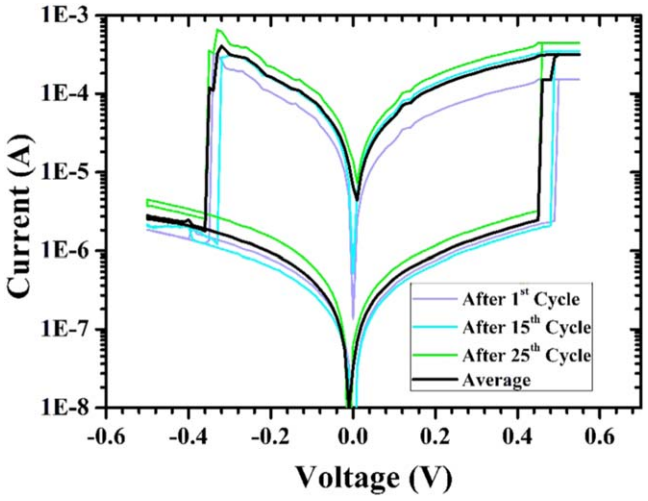

Figure 7. I–V characteristics of Al/MoS_2-GO/Al device for various cycles.

based on the migration of oxygen ions and the creation of oxygen vacancies along with the redox reaction at the electrode and formation of AlO_x at the interface. Which results in the formation of the CF formed by oxygen vacancies during the SET and but a partial dissolution of CF during the RESET consequences the gradual RESET process as shown in figure 4(d). This variation in behavior of the switching characteristics during SET and RESET attributed to the partial dissolution of the filament during the RESET are probably due to following reasons (1) random rupture of the CF during the RESET process results in fluctuation in the switching states [6]. (2) Furthermore, as cited in the past the vacancies created during the SET are not completely recovered by the Oxygen ions during RESET, leaving behind additional vacancies in the dielectric which domino effect in the partial dissolution of the CF [53]. (3) The higher concentration of oxygen ions stored in the electrode after the SET process caused thermal diffusion of oxygen ions during the RESET operation [53]. (4) The oxygen ions are easily re-oxidized by oxygen vacancies under Joule heating [54], which is related to transitions in small intermediate resistance states during the RESET process and cause the gradual RESET phenomenon.

To further study the dominating conduction and charge transport mechanism, the two types of devices were investigated through the experimental data and fitted double logarithmic plots. Figures 5(a) and (b) show the double logarithmic log(I) versus log(V) characteristics for Al/MoS_2-GO/Al and Al/MoS_2-GO/ITO structures. The slope of the curves as clearly label by fitted lines 'A, B, C, D' and 'P, Q, R, S, T' in figures 5(a) and (b). For Al/MoS_2-GO/Al device the HRS or OFF state was fitted to a straight line. For Al/MoS_2-GO/Al devices the slope is ∼1 in the entire HRS delineated by 'A' to 'B' (figure 5(a)). The switching of HRS to LRS exhibit the slope of ∼137 tagged by line 'B' to 'C'. Finally, the LRS labelled by 'C' to 'D' shows slope ∼1 (figure 5(a)). Here, the linear behaviour of I–V curves indicate ohmic conduction as described by relation ($I \propto V$). Similarly, for Al/MoS_2-GO/ITO device shows slope ∼1 in the HRS from 0 to ∼0.2 V defined by line 'P' to 'Q' (figure 5(b)), also just before the SET state, the fitted curve shows the slope ∼2 from 0.2 to 0.3 V labeled by line 'Q' to 'R' (figure 5(b)). This behaviour reveals from relation ($I \propto V^2$) and supported by the space-charge-limited conduction (SCLC). The resistance switching state (RSS) shows the slope of around 41 defined by line 'R' to 'S' (figure 5(b)). Finally, the LRS state shows slope ∼1 in line 'S' to 'T' as shown in figure 5(b). The fitted curves show slope ∼1 for Al/MoS_2-GO/Al and Al/MoS_2-GO/ITO structures, attribute to the Ohmic conduction for LRS and HRS, which designates the linear behaviour of the device in which current is proportional to voltage flows through the CF as designated in figures 5(a) and (b).

In order to investigate the electrical stabilities of the fabricated Al/MoS_2-GO/Al and Al/MoS_2-GO/ITO structures, retention tests were performed. The Al/MoS_2-GO/Al

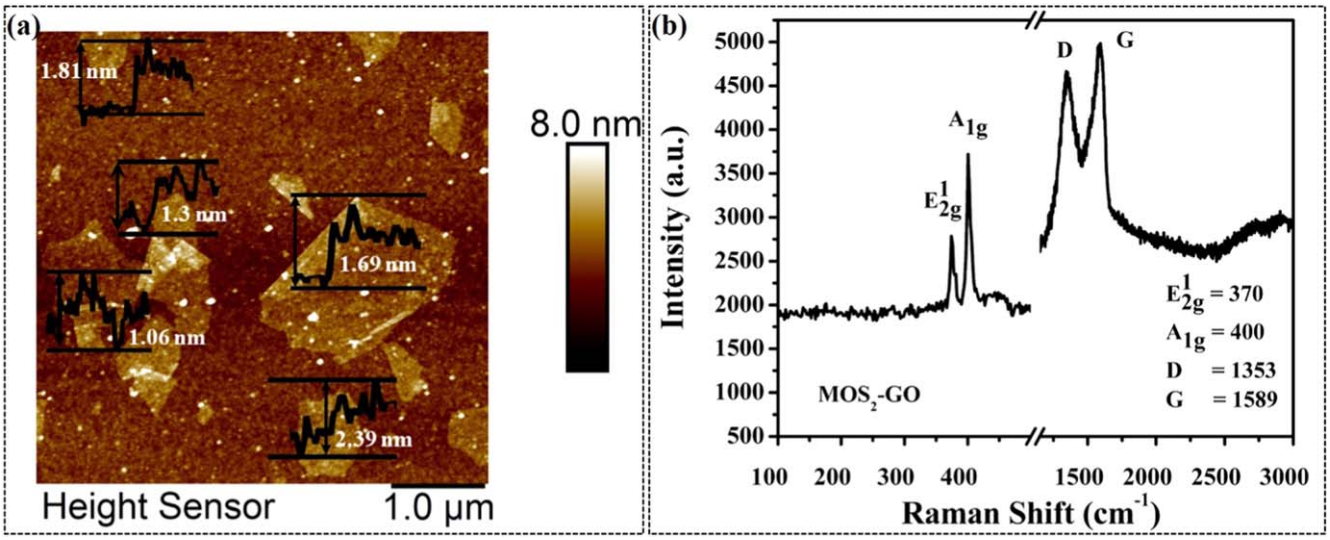

Figure 8. (a) AFM topography images of a single layer of MoS_2-GO film on the substrate along with thickness plot of MoS_2-GO nanocomposite thin film (b) micro Raman Spectroscopy profile of MoS_2-GO thin film.

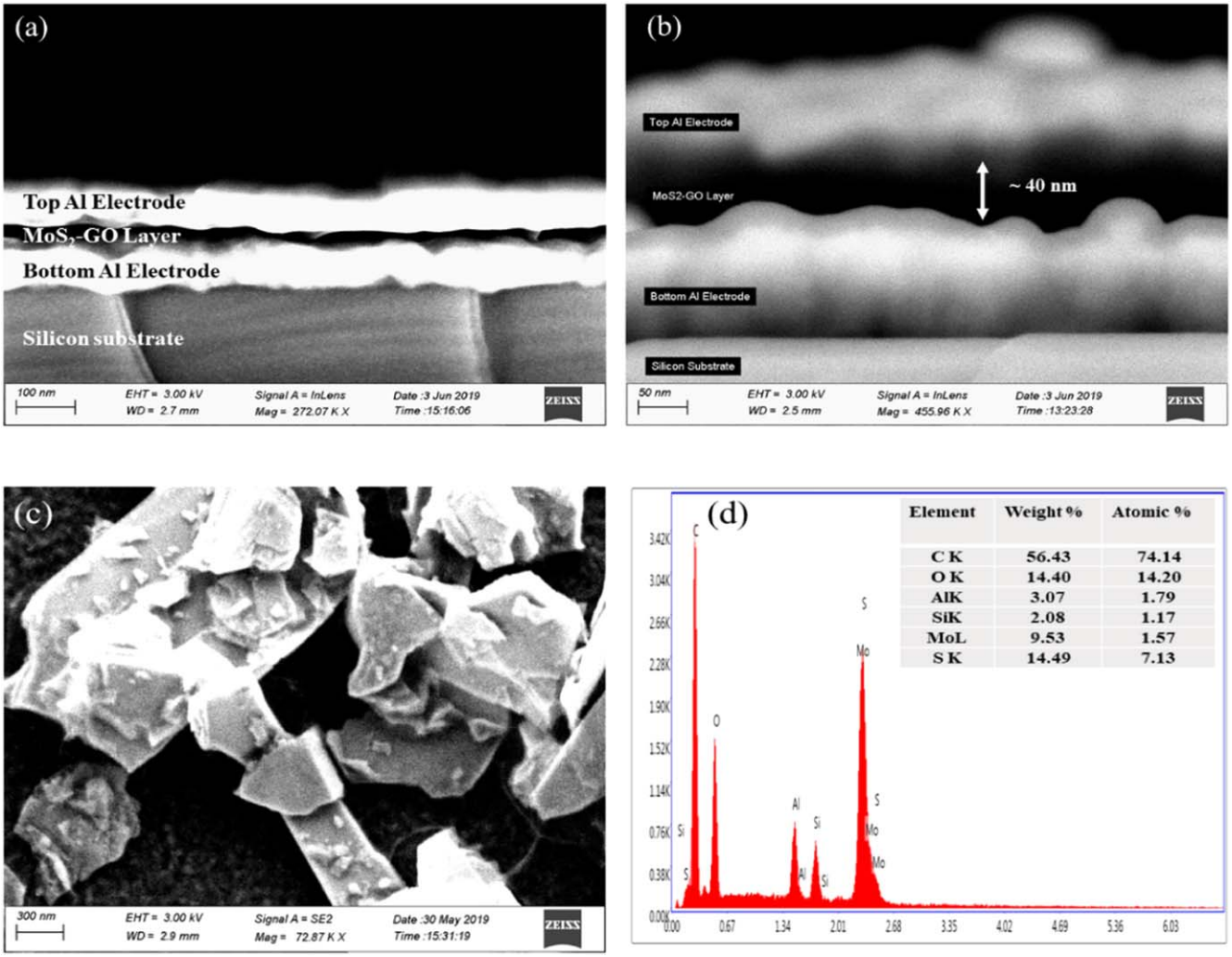

Figure 9. (a) Cross-sectional SEM of the Al/MoS_2-GO/Al device. (b) Zoomed in image for the region highlighted in figures 9(a). (c) Shows the SEM of MoS_2-GO morphology. (d) EDAX of MoS_2-GO nanocomposite.

and Al/MoS_2-GO/ITO structures subjected to retention measurements for 10^4 s at HRS as well as on LRS with a constant small reading voltage of 0.2 V. For Al/MoS_2-GO/Al devices the HRS & LRS resistance ratio is found $\sim 10^2$ while for Al/MoS_2-GO/ITO devices HRS & LRS ratio is $\sim$10 as shown in figures 6(a) and (b). As apparently perceived from MIM structures that the retention of Al/MoS_2-GO/ITO structures is one order less than counterpart whereas, both devices holds well-programmed resistance states (HRS) and (LRS) up to 10^4 s without any substantial degradation.

As clearly noticed from the I–V characteristics that Al/MoS_2-GO/Al devices exhibited robust bipolar resistive switching behavior at low operating voltages and stable retention characteristics. Hence, the I–V characteristics on the Al/MoS_2-GO/Al structures were performed repeatedly to evaluate the endurance and prove the performance of the device for real-world applications. Figure 7 shows the I–V measurements on Al/MoS_2-GO/Al structures for up to 25 cycles. The average of the 25 I–V cycles measurements were calculated and plotted in figure 7. It is clearly revealed from the characteristics that there was an insignificant variation in I–V characteristics for 25 cycles and devices behave robustly. Furthermore, Al/MoS_2-GO/Al device shows trivial dispersion in the LRS and HRS and consistently maintained the memory performance, I_{ON}/I_{OFF} ratio $\sim 10^2$ and switching voltages after 25 repetitive cycles.

Additionally, it is well established that GO has abundant hydroxyl groups and provide carbon network for electronic charge transport. Oxygen vacancies and electron traps are effortlessly generated in GO and serve as a hopping path for charge carriers transport from one electrode to another. It results in the substantial change in the resistance of the Al/MoS_2-GO /Al and Al/MoS_2-GO/ITO structures. Besides this, the presence of MoS_2 flakes as the resistive layer postulate that the smooth charge migration in the GO layer and quick change in the electrical response of the device. Because, MoS_2 flakes having a lower band gap ($\sim$1.8 eV) [24] than GO, hence contribute to increasing the conductivity of the resistive layers. Therefore, the presence of MoS_2 flakes in graphene oxide layer reduces the 'SET' voltage significantly $\sim$0.5 volts.

The surface morphology and dimensions of MoS_2-GO nanocomposite layers are confirmed with atomic force microscopy. The vertical dimensions of flakes were found between 1.06 to 2.39 nm as depicted in AFM thickness plot figure 8(a). While to confirm the chemical composition of MoS_2-GO nanocomposite resistive layers, micro-Raman spectroscopy analysis was performed at a frequency range of 200 to 3000 cm^{-1}. As depicted in figure 8(b), MoS_2-GO resistive layer exhibits four characteristic peaks. Where, first two MoS_2 peaks at $\sim$370 and $\sim$400 cm^{-1} corresponds to in-plane vibrations E^1_{2g} and out-of-plane A_{1g} vibration modes [55, 56]. Other two distinct peaks at $\sim$1353 and $\sim$1589 cm^{-1} correspond to D and G band of GO, respectively [57].

FESEM cross-sectional micrograph of device structure which clearly shows the MoS_2-GO layer is sandwiched between the top and bottom electrodes as depicted in figure 9(a). Whereas the figure 9(b) shows the magnified version of the device cross-section; the thickness of the MoS_2-GO layer was observed around $\sim$40 nm. The SEM image of the MoS_2-GO nanocomposite morphology is depicted in figure 9(c). The presence of component elements (C, O, Mo and S) in MoS_2-GO nanocomposite has been confirmed by energy dispersive X-ray spectrum EDAX analysis as shown in figure 9(d).

The performance of the fabricated Al/MoS_2-GO/Al and Al/MoS_2-GO/ITO device were compared with the state-of-the-art GO and MoS_2 as an active resistive layer memory device are summarized in table 1.

Conclusion

In summary, MoS_2-GO resistive layers have been successfully synthesized to fabricate the MIM structures. Al/MoS_2-GO/Al device show stable memory performance, I_{ON}/I_{OFF} ratios $\sim 10^2$ for more than 25 I–V cycles, the high and low resistance switching states switches below 0.5 volts and stable retention behaviour up to 10^4 s. It is to be believed that of charge hopping conduction via Al oxide defects results in low switching voltage. CF formation was occurred at the electrode interface by oxygen ion migration results in the creation of oxygen vacancies.

Acknowledgments

Authors would like to strongly acknowledge Centre for Design and Fabrication of Electronic Devices (C4DFED), Indian Institute of Technology (IIT) Mandi, India for the use of various state of the art device fabrication and characterization facilities for present work. This work was financially supported by the project Ref No: SCSTE/F(8)-1/2016, Indian Institute of Technology (IIT), Mandi, (H.P), India. Author Sumit Choudhary would like to thank 'Visvesvaraya PhD scheme' from MeitY, Govt. of India for the research fellowship.

ORCID iDs

Sumit Choudhary https://orcid.org/0000-0002-3127-4691
Satinder K Sharma https://orcid.org/0000-0001-9313-5550

References

[1] Waser R, Dittmann R, Staikov G and Szot K 2009 Redox-based resistive switching memories–nanoionic mechanisms, prospects, and challenges *Adv. Mater.* **21** 2632–63
[2] Mazumder P, Kang S-M and Waser R 2012 Memristors: devices, models, and applications *Proc. IEEE* **100** 1911–9

[3] Chang T, Chang K, Tsai T, Chu T and Sze S M 2016 Resistance random access memory *Biochem. Pharmacol.* **19** 254–64

[4] Sharma A K 2009 *Advanced Semiconductor Memories: Architectures, Designs, and Applications* (USA: Wiley-IEEE Press) 0470528370 9780470528372

[5] Liu M, Xia L, Wang Y and Chakrabarty K 2019 Fault tolerance in neuromorphic computing systems *Proc. of the 24th Asia and South Pacific Design Automation Conf. (ACM)* 216–223

[6] Abbas H, Ali A, Jung J, Hu Q, Park M R, Lee H H, Yoon T-S and Kang C J 2019 Reversible transition of volatile to non-volatile resistive switching and compliance current-dependent multistate switching in IGZO/MnO RRAM devices *Appl. Phys. Lett.* **114** 93503

[7] Nagareddy V K, Barnes M D, Zipoli F, Lai K T, Alexeev A M, Craciun M F and Wright C D 2017 Multilevel ultrafast flexible nanoscale nonvolatile hybrid graphene oxide–titanium oxide memories *ACS Nano* **11** 3010–21

[8] Huang R, Yan X, Ye S, Kashtiban R, Beanland R, Morgan K A, Charlton M D B and de Groot C H K 2017 Resistive memory with controllable interfacial multistate switching behaviour *Nanoscale Res. Lett.* **12** 384

[9] Abbas H, Abbas Y, Truong S N and Min K 2017 A memristor crossbar array of titanium oxide for non-volatile memory and neuromorphic applications *Semicond. Sci. Technol.* **32** 065014

[10] Hu Q, Ra M, Abbas H, Su T, Yoon T and Jung C 2018 Forming-free resistive switching characteristics in tantalum oxide and manganese oxide based crossbar array structure *Microelectron. Eng.* **190** 7–10

[11] Lee J-S 2011 Progress in non-volatile memory devices based on nanostructured materials and nanofabrication *J. Mater. Chem.* **21** 14097–112

[12] Jeong H Y, Kim J Y, Kim J W, Hwang J O, Kim J-E, Lee J Y, Yoon T H, Cho B J, Kim S O and Ruoff R S 2010 Graphene oxide thin films for flexible nonvolatile memory applications *Nano Lett.* **10** 4381–6

[13] Panin G N, Kapitanova O O, Lee S W, Baranov A N and Kang T W 2011 Resistive switching in Al/graphene oxide/Al structure *Jpn. J. Appl. Phys.* **50** 70110

[14] Pantel D, Goetze S, Hesse D and Alexe M 2011 Room-temperature ferroelectric resistive switching in ultrathin Pb($Zr_{0.2}Ti_{0.8}$)O_3 films *ACS Nano* **5** 6032–8

[15] Li Y, Zhong Y, Xu L, Zhang J, Xu X, Sun H and Miao X 2013 Ultrafast synaptic events in a chalcogenide memristor *Sci. Rep.* **3** 1619

[16] Yang C-H, Seidel J, Kim S Y, Rossen P B, Yu P, Gajek M, Chu Y-H, Martin L W, Holcomb M B and He Q 2009 Electric modulation of conduction in multiferroic Ca-doped BiFeO 3 films *Nat. Mater.* **8** 485

[17] Chen X G, Ma X B, Yang Y B, Chen L P, Xiong G C, Lian G J, Yang Y C and Yang J B 2011 Comprehensive study of the resistance switching in $SrTiO_3$ and Nb-doped $SrTiO_3$ *Appl. Phys. Lett.* **98** 122102

[18] Maksymovych P, Jesse S, Yu P, Ramesh R, Baddorf A P and Kalinin S V 2009 Polarization control of electron tunneling into ferroelectric surfaces *Science (80-.)* **324** 1421–5

[19] Novoselov K S, Geim A K, Morozov S V, Jiang D A, Zhang Y, Dubonos S V, Grigorieva I V and Firsov A A 2004 Electric field effect in atomically thin carbon films *Science (80-.)* **306** 666–9

[20] Chhowalla M, Shin H S, Eda G, Li L-J, Loh K P and Zhang H 2013 The chemistry of two-dimensional layered transition metal dichalcogenide nanosheets *Nat. Chem.* **5** 263

[21] Tan C, Liu Z, Huang W and Zhang H 2015 Non-volatile resistive memory devices based on solution-processed ultrathin two-dimensional nanomaterials *Chem. Soc. Rev.* **44** 2615–28

[22] Li X and Zhu H 2015 Two-dimensional MoS_2: properties, preparation, and applications *J. Mater.* **1** 33–44

[23] Deng Y, Luo Z, Conrad N J, Liu H, Gong Y, Najmaei S, Ajayan P M, Lou J, Xu X and Ye P D 2014 Black phosphorus–monolayer MoS_2 van der Waals heterojunction p–n diode *ACS Nano* **8** 8292–9

[24] Wang W, Panin G N, Fu X, Zhang L, Ilanchezhiyan P, Pelenovich V O, Fu D and Kang T W 2016 MoS_2 memristor with photoresistive switching *Sci. Rep.* **6** 31224

[25] Wager J F 2003 Transparent electronics *Science (80)* **300** 1245–6

[26] Soni M, Soni A and Sharma S K 2018 Integration of graphene oxide buffer layer/graphene floating gate for wide memory window in Pt/Ti/Al_2O_3/GO/graphene/SiO_2/p-Si/Au non-volatile (FLASH) applications *Appl. Phys. Lett.* **112** 252102

[27] Lin K-L, Hou T-H, Shieh J, Lin J-H, Chou C-T and Lee Y-J 2011 Electrode dependence of filament formation in HfO_2 resistive-switching memory *J. Appl. Phys.* **109** 084104

[28] Cartoixà X, Rurali R and Suñé J 2012 Transport properties of oxygen vacancy filaments in metal/crystalline or amorphous HfO_2/metal structures *Phys. Rev.* B **86** 165445

[29] Yang J J, Pickett M D, Li X, Ohlberg D A A, Stewart D R and Williams R S 2008 Memristive switching mechanism for metal/oxide/metal nanodevices *Nat. Nanotechnol.* **3** 429

[30] Paulchamy B, Arthi G and Lignesh B D 2015 A simple approach to stepwise synthesis of graphene oxide nanomaterial *J. Nanomed. Nanotechnol.* **6** 253

[31] Soni M, Arora T, Khosla R, Kumar P, Soni A and Sharma S K 2016 Integration of highly sensitive oxygenated graphene with aluminum micro-interdigitated electrode array based molecular sensor for detection of aqueous fluoride anions *IEEE Sens. J.* **16** 1524–31

[32] Soni M, Kumar P, Pandey J, Sharma S K and Soni A 2018 Scalable and site specific functionalization of reduced graphene oxide for circuit elements and flexible electronics *Carbon N. Y.* **128** 172–8

[33] Lütz G 2007 *Semiconductor Radiation Detectors: Device Physics* (Heidelberg: Springer) (https://doi.org/10.1007/978-3-540-71679-2)

[34] Sun X, Sun B, Liu L, Xu N, Liu X, Han R, Kang J, Xiong G and Ma T P 2009 Resistive switching in CeO_x films for nonvolatile memory application *IEEE Electron Device Lett.* **30** 334–6

[35] Zou L, Hu W, Fu J, Qin N, Li S and Bao D 2014 Uniform bipolar resistive switching properties with self-compliance effect of Pt/TiO_2/p-Si devices *AIP Adv.* **4** 037106

[36] Lee D, Woo J, Park S, Cha E and Lee S 2014 Dependence of Reactive Metal Layer on Resistive Switching in a Bi-layer Structure Ta/HfOx Filament Type Resistive Random Access Memory *Appl. Phys. Lett.* **104** 083507

[37] Li S *et al* 2013 Bipolar resistive switching behavior with high ON/OFF ratio of Co: $BaTiO_3$ films by acceptor doping *Appl. Phys. Lett.* **102** 153506

[38] Lee K-J, Wang L-W, Chiang T-K and Wang Y-H 2015 Effects of electrodes on the switching behavior of strontium titanate nickelate resistive random access memory *Materials (Basel).* **8** 7191–8

[39] Rahaman S Z and Maikap S 2013 Comparison of resistive switching characteristics using copper and aluminum electrodes on GeO x/W cross-point memories *Nanoscale Res. Lett.* **8** 509

[40] Hong S K, Kim J E, Kim S O, Choi S-Y and Cho B J 2010 Flexible resistive switching memory device based on graphene oxide *IEEE Electron Device Lett.* **31** 1005–7

[41] Zhao F *et al* 2012 Chemoselective photodeoxidization of graphene oxide using sterically hindered amines as catalyst: synthesis and applications *ACS Nano* **6** 3027–33

[42] He C L, Zhuge F, Zhou X F, Li M, Zhou G C, Liu Y W, Wang J Z, Chen B, Su W J and Liu Z P 2009 Nonvolatile resistive switching in graphene oxide thin films *Appl. Phys. Lett.* **95** 232101

[43] Yin Z, Zeng Z, Liu J, He Q, Chen P and Zhang H 2013 Memory Devices Using a Mixture of MoS_2 and Graphene Oxide as the Active Layer *Small* **9** 727–731
[44] Tan C *et al* 2015 Self-assembled chiral nanofibers from ultrathin low-dimensional nanomaterials *J. Am. Chem. Soc.* **137** 1565–71
[45] Liu J, Zeng Z, Cao X, Lu G, Wang L, Fan Q, Huang W and Zhang H 2012 Preparation of MoS_2-polyvinylpyrrolidone nanocomposites for flexible nonvolatile rewritable memory devices with reduced graphene oxide electrodes *Small* **8** 3517–22
[46] Chen C, Song C, Yang J, Zeng F and Pan F 2012 Oxygen migration induced resistive switching effect and its thermal stability in W/TaO x/Pt structure *Appl. Phys. Lett.* **100** 253509
[47] Lorenzi P, Rao R and Irrera F 2013 Forming kinetics in HfO_2-based RRAM Cells *IEEE Trans. Electron Devices* **60** 438–43
[48] Gao B, Sun B, Zhang H, Liu L, Liu X, Han R, Kang J and Yu B 2009 Unified physical model of bipolar oxide-based resistive switching memory *IEEE Electron Device Lett.* **30** 1326–8
[49] Russo U, Ielmini D, Cagli C and Lacaita A L 2009 Filament conduction and reset mechanism in NiO-based resistive-switching memory (RRAM) devices *IEEE Trans. Electron Devices* **56** 186–92
[50] Rahaman S Z, Maikap S, Chen W S, Lee H Y, Chen F T, Kao M J and Tsai M J 2012 Repeatable unipolar/bipolar resistive memory characteristics and switching mechanism using a Cu nanofilament in a GeOx film *Appl. Phys. Lett.* **101** 73106
[51] Waser R and Aono M 2010 Nanoionics-based resistive switching memories *Nanoscience And Technology: A Collection of Reviews from Nature Journals* (Singapore: World Scientific) pp 158–65
[52] Kim S, Choi S and Lu W 2014 Comprehensive physical model of dynamic resistive switching in an oxide memristor *ACS Nano* **8** 2369–76
[53] Sarkar B, Lee B and Misra V 2015 Understanding the gradual reset in $Pt/Al_2O_3/Ni$ RRAM for synaptic applications *Semicond. Sci. Technol* **30** 105014
[54] Zhong C *et al* 2013 Effect of ITO Electrode with different oxygen contents on the electrical characteristics of HfOx RRAM devices *Surface & Coatings Technology* **231** 563–6
[55] Lee C, Yan H, Brus L E, Heinz T F, Hone J and Ryu S 2010 Anomalous lattice vibrations of single-and few-layer MoS_2 *ACS Nano* **4** 2695–700
[56] Li H, Zhang Q, Yap C C R, Tay B K, Edwin T H T, Olivier A and Baillargeat D 2012 From bulk to monolayer MoS_2: evolution of Raman scattering *Adv. Funct. Mater.* **22** 1385–90
[57] Stankovich S, Dikin D A and Piner R D 2007 Synthesis of graphene-based nanosheets via chemical reduction of exfoliated graphite oxide *Carbon* **45** 1558–65